Winter cascading of cold water in Lake Geneva

Ilker Fer[1] and Ulrich Lemmin
Laboratoire de Recherches Hydrauliques, Ecole Polytechnique Fédérale de Lausanne, Lausanne, Switzerland

S. A. Thorpe
School of Ocean and Earth Science, Southampton Oceanography Centre, Southampton, UK

Received 2 February 2001; revised 16 October 2001; accepted 6 November 2001; published 27 June 2002.

[1] During the winters of 1998 and 1999, observations were made of the cascading of cold water from the nearshore, shallow "shelf" zones and down the sloping sides of Lake Geneva. Cascading starts on the average 10 hours after the onset of surface cooling. The draining cold water descends like a gravity current, and the downslope speed of the head of these slugs of cold water, U, has a mean value of 5.2 cm s^{-1}, with slugs persisting, on the average, for 8 hours. When the Monin-Obukov length scale at the water surface, L, is negative, implying convection occurs, and $\overline{d}/|L| > 1$, where $\overline{d}$ is the mean shelf depth, the nondimensionalized speed of the front of "slugs," $U/b^{1/3}$ is found to be 1.3 ± 0.4, where b is the surface buoyancy flux integrated over the time period from one slug to the next. Each slug is unsteady, the head being followed by several fronts in which the temperature of the current decreases and its thickness increases. These fronts travel faster than the mean flow by a factor of $r = 1.38 \pm 0.3$. Dynamical similarities are found with roll waves observed in turbulent open channel flows. The circulation induced by the cascade is found to give a positive skewness to the time derivatives of near-surface temperature in shallow waters, in contrast with negative values close to the slope. The volume of cold water carried by a slug increases with downslope distance as a consequence of turbulent entrainment and the contribution of convectively unstable plumes from the surface. The average volume carried by the slug across the 21 m depth contour is about 1.9 times the volume of water in shallower water (i.e., that on the shelf between shore and a depth of 21 m), implying that cascading is an efficient means of flushing shelf water. Integrated around the lake the mean total volume flux amounts to 11.5 the average winter river inflow. *INDEX TERMS:* 4239 Oceanography: General: Limnology; 4227 Oceanography: General: Diurnal, seasonal, and annual cycles; 3020 Marine Geology and Geophysics: Littoral processes;
KEYWORDS: lake, shelf, convective processes, dense water, cascade, gravity current

1. Introduction

[2] During periods of winter cooling the temperature of the shallow well-mixed waters at the edges of lakes or that of continental shelves surrounding the ocean basins falls more rapidly than that of adjacent deeper waters, provided that the heat loss from the water surface is relatively uniform. This resulting spatial temperature variation leads to the formation of a relatively cold and dense bottom layer in the shallows, which flows or cascades down the sides of lakes or the continental slopes in the form of gravity currents.

[3] There have been several observations of "winter cascading" in the ocean. *Cooper and Vaux* [1949], who appear to have invented the term, used measurements of salt, temperature, oxygen, and pH to demonstrate the phenomena had occurred from the U.K. Celtic Sea shelf in the winter of 1913–1914. They also suggested that the submarine banks and valleys of the Celtic Sea were likely to exert considerable control over the currents initiated by the cascade. *Tomczak* [1985] used conductivity-temperature-depth (CTD) measurements to show that the shallow Bass Strait water entered the deeper Tasman Sea in significant quantities during the winter of 1981. *Hill et al.* [1998] made measurements with a CTD instrument equipped with a fluorometer, transmissometer, and sampling bottles to describe a dense 20–50 m thick plume over the continental slope northwest of Ireland, which penetrated to a depth of 500 m. Several observers, including *Muench and Gordon* [1995] and *Fahrbach et al.* [1995], have made CTD profiles around Antarctica. A thorough review of their observations and modeling of the Antarctic downslope flows is given by *Baines and Condie* [1998]. They divide the data in those that show plumes apparently occurring during the time of observation and those that had previously originated on the continental shelf. They emphasize the effects of Coriolis

[1]Now at Geophysical Institute, University of Bergen, Bergen, Norway.

Copyright 2002 by the American Geophysical Union.
0148-0227/02/2001JC000828$09.00

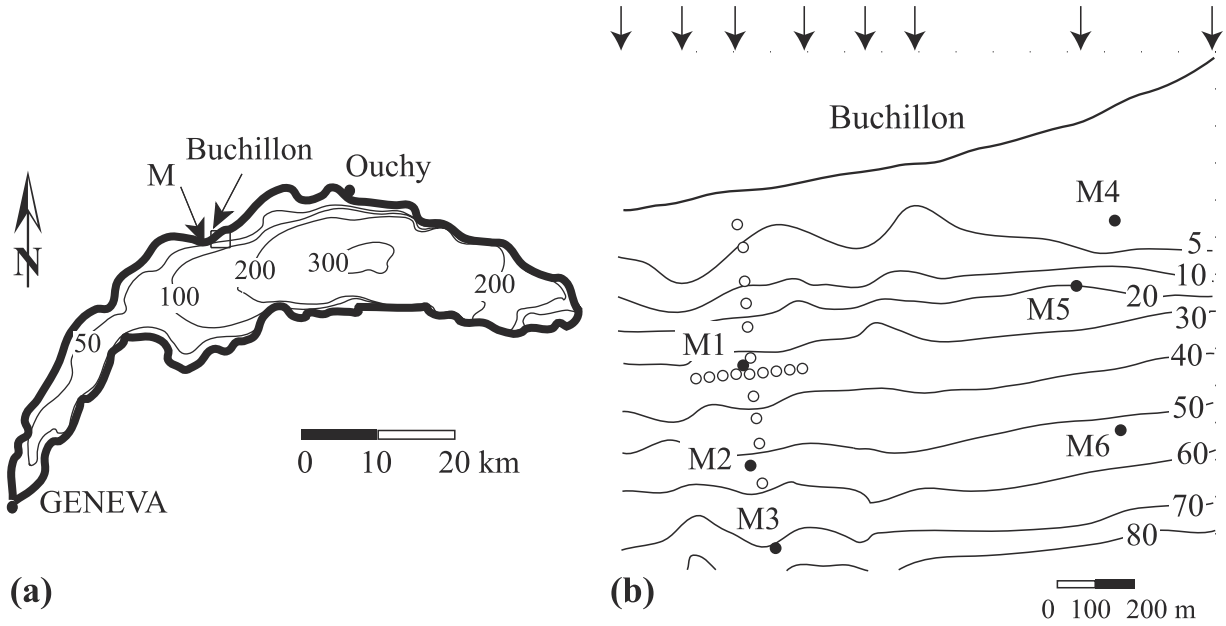


Figure 1. (a) Bathymetric map of Lake Geneva. (b) The box is enlarged to show sampling locations of the experiments. Depth contours are in meters. M is the location of the meteorological mast. The isobaths in Figure 1b are derived from repeated north-south transects carried out in the lines indicated by arrows, using an echosounder and GPS. The solid dots in Figure 1b show the vertical moorings. M1 is deployed above the 30 m isobath and includes four temperature miniloggers at 5 m intervals. M2 and M3 are deployed above the 56 and 71 m isobaths and include 11 thermistors at 2.5 and 5 m intervals. The moorings M4, M5, and M6 include 5, 12, and 8 thermistor miniloggers and are deployed above 5, 21, and 55 m depth contours, respectively. The open circles mark thermistor miniloggers laid on the bottom.

forces, which lead to mainly alongslope flows with downslope drainage in bottom Ekman layers.

[4] The flow of dense water down slopes has been studied in laboratory conditions for both nonrotating flows [*Ellison and Turner*, 1959; *Britter and Linden*, 1980; *Alavian*, 1986] and rotating flows [*Smith*, 1977; *Whitehead et al.*, 1990; *Condie*, 1995; *Zatsepin et al.*, 1996; *Lane-Serff and Baines*, 1998]. The experiments on nonrotating flows cover ranges of about $50 < Re < 2500$, $0.1 < Fr' < 25$, and $0° \leq \beta \leq 90°$. Here Re is the flow Reynolds number, uh/v, where u is the flow speed and h is the thickness of the dense layer and v is the kinematic viscosity. Fr' is the internal Froude number, $u^2/g' h$, where g' is the reduced acceleration of gravity of the dense layer, and β is the slope angle. In experiments with rotation the downslope flow is deflected by Coriolis forces. Several experimenters report the development of waves with crests orientated across the mean current flow (e.g., Ellison and Turner and Alavian in nonrotating systems; Zatsepin et al., Whitehead, and Lane-Serff and Baines in rotating flows). *Zatsepin et al.* [1996] report that the waves appear at values of $Fr' > 2.3$ when $2 < Re < 50$.

[5] There have also been some studies of the circulation produced by cooling in lakes. *Sturman et al.* [1999] have made measurements using thermistor chains and an acoustic Doppler velocity profiler (ADCP) to describe the nearshore circulation in shallow lakes, in depths of about 3 m. They find that surface cooling drives a surface flow toward shore and a relatively colder layer offshore. Others have studied the "thermal bar" when the temperature falls below that of the maximum water density at 4°C [e.g., see *Zilitinkevich et al.*, 1992]. We shall not comment further about this phenomenon because temperatures were above 4°C in all our observations.

[6] Our studies are made in the 315 m deep Lake Geneva. In previous observations during periods of winter cooling in Lake Geneva near Ouchy (see Figure 1a), *Thorpe et al.* [1999] reported a layer of cold water with a thickness of the order of 10 m adjacent to the sloping boundary of the lake, which on reaching the thermocline, spreads as an intrusion. "Plumes" of relatively cold water, typically 5 m wide and 20 m apart, are found in the near-surface convective mixed layer when air temperatures are 7°C below the surface water temperature. Turbulence is enhanced in the cold slope boundary layer, where the dissipation rate of turbulent kinetic energy is about 1 order of magnitude greater than those distant from the slope [*Fer et al.*, 2002]. Earlier analysis of idealized two-layer profiles of temperature together with current measurements shows that there is a balance between buoyancy force and drag such that $C_D \overline{u}^2 = g' h \sin \beta$, with a drag coefficient, C_D, estimated to be $(4 \pm 0.7) \times 10^{-3}$ [*Fer et al.*, 2000]. Here g' is the reduced gravity, h is the thickness of the cold boundary layer, β is the bottom slope angle, and $\overline{u}$ is the mean downslope flow. Evidence of winter cascading in Lake Geneva has also been found at Buchillon [*Fer et al.*, 2001]. Cascading is observed to be periodic on two timescales. It occurs on a 24 hour period in response to diurnal heating and cooling, with downslope flows or "slugs" of cold water, each preceded by a head or temperature front structure and lasting for some 8 hours. However, as observed in the laboratory flows, the slugs are subject to waves or pulsing; the slug flow is

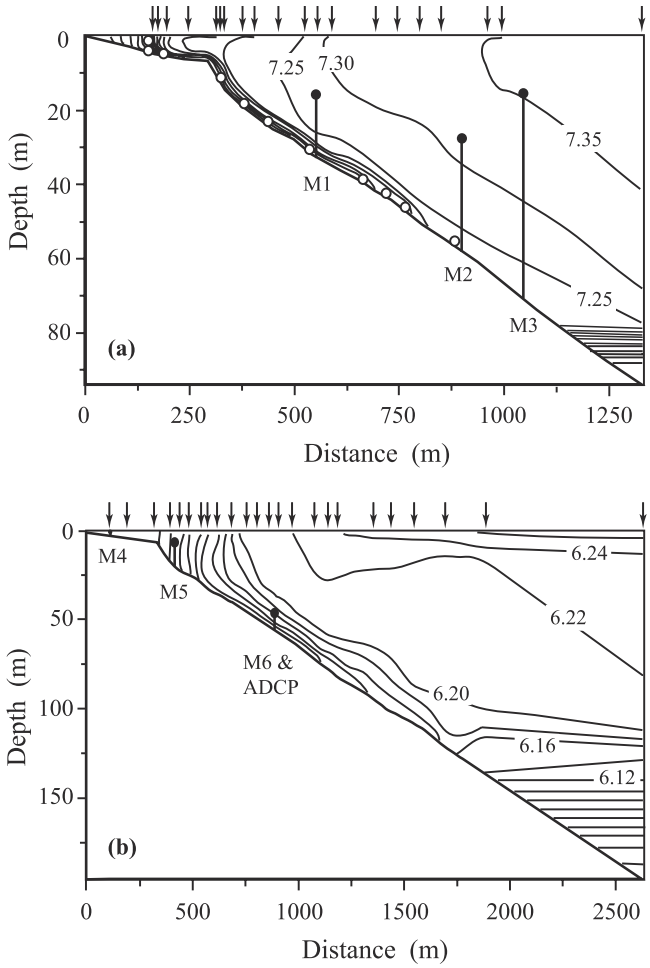


Figure 2. Isotherms derived from CTD profilings conducted between (a) 1030 and 1330 LT, 23 December 1998, during experiment I and (b) 1200 and 1500 LT, 20 January 2000, during experiment II. The contours are in degrees Celsius. The profiling stations are indicated by arrows. Open circles in Figure 2a show the temperature miniloggers laid at the bottom, as well as the one 2 m off the bottom at 4 m depth. Vertical moorings deployed during the experiments are shown as M1–M6.

observed to contain thermal "fronts" moving faster than the mean flow marking the arrival of colder water. Pulses occur at about 3 hour intervals.

[7] Here we describe further observations made at Buchillon (see Figure 1a) with the objective of establishing and quantifying the nature (particularly the diurnal cycle) and the effect of winter cascading. The site and methodology are described in section 2. Observations are presented and analyzed in section 3. Results are discussed in section 4 and interpreted in light of the laboratory experiments and available theory. Conclusions are summarized in section 5.

2. Site, Experiments, and Environmental Forcing

[8] The measurements described below were made in the vicinity of Buchillon, on the northern shore of Lake Geneva, during the winter of 1998–1999 (experiment I) and 1999–2000 (experiment II). A bathymetric map is shown in Figure 1. (This includes the mooring locations of the experiments.) The isobaths are aligned approximately in the east-west direction. The bottom slope of the area is derived from repeated transects carried out in the offshore direction using an echosounder and GPS. The mean slope values are 1° out to 7 m depth, providing a relatively wide shallow water shelf extending some 0.25 km from shore, a steep slope of 20° between 7 and 15 m, and a slope of 4.6° between 15 and 80 m depth.

[9] Wind speed and direction, air temperature, shortwave radiation, humidity, and air pressure were recorded every 5 min at a meteorological mast located at M in Figure 1a. Because of orographic constraints, the wind field over the lake is dominated by NE and SW winds. During 55% of the total observation period, wind speed was <3 m s^{-1}. Out of a total of 92 days of observation a diurnal pattern of cooling and heating with typically 5 hour periods of daytime warming interrupting the longer periods of cooling occurred on 64 days. Net surface heat flux H is calculated using bulk aerodynamic formulae [*Fischer et al.*, 1979]. The surface buoyancy flux B is calculated as $B = -g\alpha H/(C_p\rho_o)$, where α is the coefficient of thermal expansion of water, C_p is the specific heat of water, and ρ_o is the density of water. The nighttime air temperatures, typically some 6°C below the lake surface temperature, led to a mean surface buoyancy flux from the lake to the air of $B = (2.3 \pm 1.1) \times 10^{-8}$ m^2 s^{-3} (henceforth, ± represents the standard deviation of the observed values). The positive value of B implies that the lake loses heat and buoyancy. The Monin-Obukov length scale L in the water was calculated as $L = -u_*^3/\kappa B$. The friction velocity in the water, u_*, is estimated by supposing that the wind stress is balanced by the stress in the water surface and $\kappa = 0.4$ is the von Karman constant. The mean value of L was $-(2.5 \pm 6.3)$ m during cooling periods implying that on the average, convection free of mechanical mixing occurred at depths exceeding about $-2L$, or 5 m [*Shay and Gregg*, 1986]. Uncertainties in the values of B and L are derived from the errors in calculating the net surface heat flux H and the friction velocity u_* and are estimated to be 10 and 15%, respectively. Errors in calculating H include the errors in measuring air and surface water temperature, the wind speed, and the shortwave radiation. The errors in u_* result from errors in measuring the wind speed and calculating the drag coefficient.

[10] Occasional CTD profiles made along sections normal to the shoreline near the mooring lines added ancillary information throughout the experiment periods. The CTD sensors sample at 4.5 Hz, and the resolution of the temperature sensor is 0.001°C. The instrument lowering speed was ~10 cm s^{-1}. During both experiments, recorded currents are converted to downslope, normal to the isobaths, and alongslope components, and the Aanderaa thermistor chains and the miniloggers described below sampled every 5 min to 0.05°C resolution and every 2.5 min to 0.015°C, respectively. Aanderaa current meters sampled every 5 min.

2.1. Experiment I, Winter 1998–1999

[11] Experiment I covers 54 days of observation starting from 7 November 1999. The positions of the instruments are shown in Figure 1b (see also Figure 2a for a vertical cross section). Two vertical Aanderaa thermistor chains were deployed above 56 (M2) and 71 m (M3) depth

contours with a horizontal separation of 200 m. Each vertical chain had 11 thermistors with vertical separations of 2.5 and 5 m, respectively. A downslope line of 11 self-contained temperature miniloggers was laid along a line close to the north-south direction (Figure 1b). Each minilogger was supported by a buoyant collar, keeping the temperature sensor at a height of 0.5 m off the bottom. The downslope separations between the sensors were 23, 144, 68, 100, 73, 83, 65, 60, and 108 m, respectively. A second linear array of nine miniloggers with 30 m spacing was deployed along slope at the bottom, following depth contours of 35 m. An additional vertical array of four temperature miniloggers was deployed above the 30 m isobath, with vertical separations of 5 m (M1). An Aanderaa current meter at M2, 2 m above the bottom, provided essential information about the bottom current. Miniloggers laid on the bottom at 5, 10, 17.4, and 23 m isobaths recorded until 15 December 1998 when they were inadvertently recovered by fishermen.

[12] Isotherms derived from CTD profiles on 23 December 1998 are shown in Figure 2a. After overnight or longer periods of cooling, a layer of relatively cold water, with thickness h of 2–15 m is found on the slope between the shallows and the thermocline depth D, typically at 80–150 m. Similar cold bottom boundary layers, typically 5–10 m thick and 0.1 K lower in temperature than the overlying water, commonly occur on the 5°–20° lateral slopes of the lake at depths shallower than that of the thermocline [*Thorpe et al.*, 1999; *Fer et al.*, 2000, 2001, 2002]. The cold layer adjacent to the slope appears to be a slug of cold water advancing downslope.

2.2. Experiment II, Winter 1999–2000

[13] During the second experiment, measurements were made for 38 days from 30 December 1999 onward. Vertical moorings consisting of self-contained temperature miniloggers were deployed above 5 (M4), 21 (M5), and 55 m (M6) depth contours covering ranges of 0.5–4.2, 1.2–15, and 1.2–7.2 m above the bottom, respectively (for positions, see Figure 1b and Figure 2b). The horizontal separation between M5 and M6 is ~500 m. Currents were measured with three Aanderaa current meters, two deployed at M5 (2 and 4 m above the bottom) and one at M6 (2 m off the bottom). An additional upward looking RD Instruments workhorse broadband ADCP was installed at the bottom at M6, profiling a vertical range from 5 to 50 m off the bottom, with 2 m bins. The system frequency of the ADCP is 300 kHz, and for the depth cells of size 2 m this leads to a precision of 4 cm s^{-1}. Continuous profile recording was averaged over 6 min intervals.

[14] The isotherms given in Figure 2b are derived from CTD profiles on 20 January 2000. The cold plume near the slope is the remains of the slug detected by the minilogger array during the morning of the day.

3. Observations

3.1. General Properties of the Cascade Flow

3.1.1. Structure of individual slugs

[15] An example of two slugs traveling down the slope during the surface cooling periods of 20–21 January 2000 is shown in Figure 3. Figure 3a shows the surface buoyancy flux. The shaded band indicates the period when the CTD profiles were taken (Figure 2b). Contours from vertical arrays of thermistors at M4, M5, and M6 are given in Figures 3b–3d. The parts corresponding to the slugs are shaded. Slugs arrive sequentially at M5 and M6, and the thickness of the slug at M5 increases some 4 hours after its first arrival. The cold bottom layer in Figure 2b, taken from data collected on 20 January, is the end of the slug that developed during the night of 19 January. The across-slope, u (thick line), and alongslope, v (thin line), components of currents measured 2 m off the bottom at M6 are given in Figure 3e. The arrows show the periods of downslope flow associated with the cold water slugs. The slugs are sometimes associated with high acoustic scattering recorded by the ADCP, particularly noticeable in Figure 3f on 22 January, suggesting a relatively higher suspended sediment concentration, although this cannot presently be quantified. Conditional sampling of the ADCP data for the periods of cooling in experiment II shows that the high acoustic scattering correlates with downslope speeds u exceeding 6 cm s^{-1}; there is a correlation coefficient of 0.5 between these speeds and the scattering intensity.

3.1.2. Volume and buoyancy flux

[16] Data from experiment II are examined to describe the dynamics of cold water slugs associated with the winter cascade. The current meters and temperature sensors at moorings M5 and M6 as well as the ADCP at M6 allow estimates to be made of volume flux q and buoyancy flux B_s of the slugs per unit alongslope length.

[17] The thickness of the slug, h, at M5 is estimated as that of the bottom layer in which the temperature θ is lower than the ambient temperature θ_{amb}, calculated as the mean temperature recorded by the topmost sensors of both vertical arrays at M5 and M6 over the 30 min period before the slug starts. Since the vertical thermistor array at M6 is too short for such estimates, h is taken as the height where the downslope speed u recorded by the ADCP was zero. This gives an estimation of the slug thickness to a 2 m resolution in vertical. In the calculation of the volume and buoyancy fluxes at M6 this would not have a significant effect because of the low downslope velocities close to the upper boundary of the slug. At M5 the downslope flow u recorded by the 2 m off-bottom current meter is used, while at M6 a vertical profile of u is obtained by the ADCP. Time-integrated buoyancy flux B_s and average volume flux q of the slugs are estimated by integrals given in equations (1) and (2), respectively, using the measured time series of u and θ and the estimated values of h and θ_{amb}:

$$B_s = g\alpha \int_T \int_0^{z \text{ at } u=0} (\theta_{amb} - \theta)\, u dz dt, \tag{1}$$

$$q = \frac{1}{T} \int_T \int_0^{z \text{ at } u=0} u dz dt. \tag{2}$$

In equation (1), g is the acceleration of gravity; α is the coefficient of thermal expansion, 4.6×10^{-5}°C^{-1} at 7°C; T is the total duration of a slug; and z is the vertical distance normal to the slope.

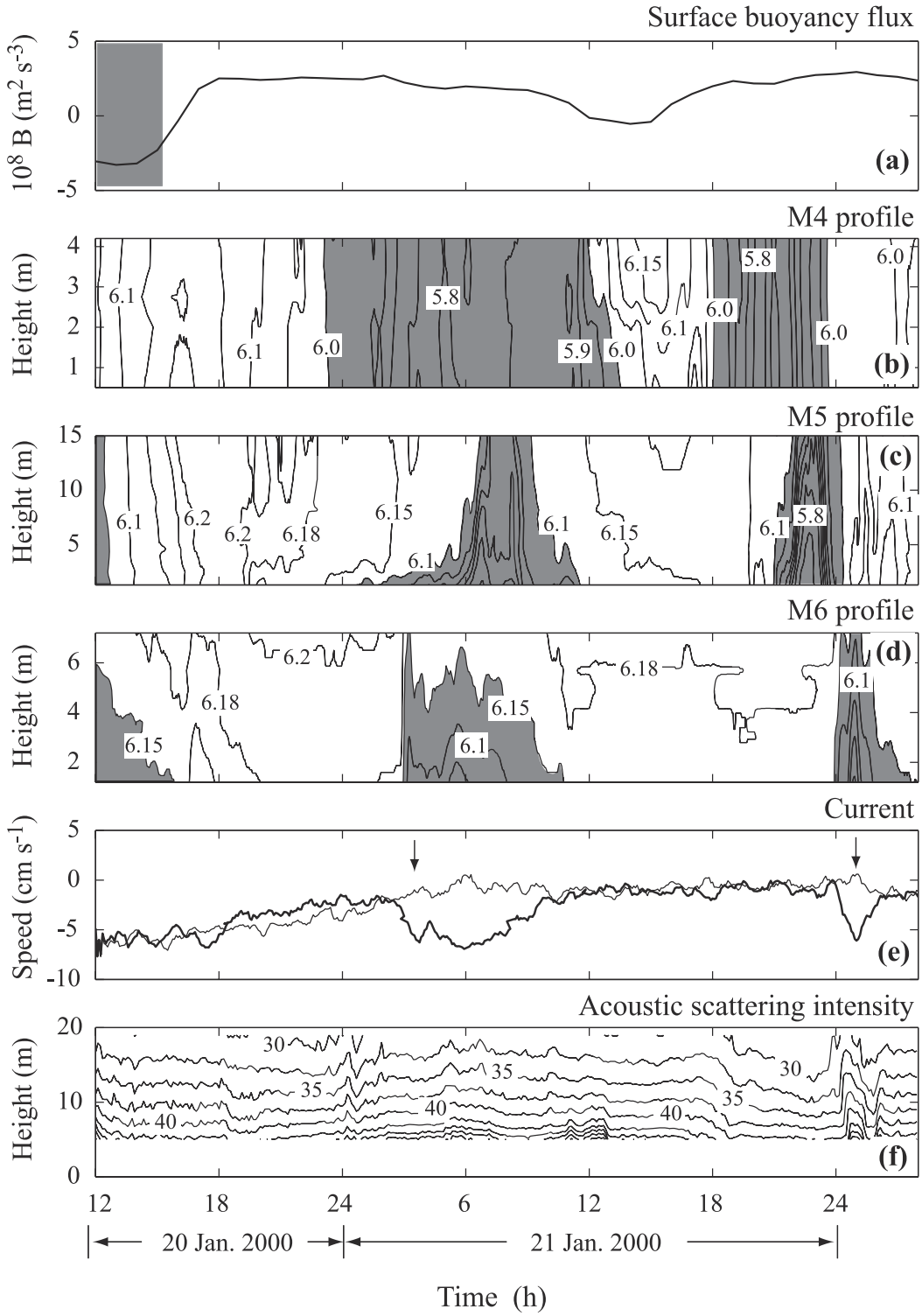


Figure 3. The movement of cold water slugs down the slope. (a) Hourly averaged values of the surface buoyancy flux B. The mean Monin-Obukov length scale L is -0.9 ± 0.6 m. The shaded band is the period when the CTD profiling was made (see Figure 2b). (b), (c), and (d) Half-hourly smoothed isotherms derived from the time series of temperature recorded by vertical arrays at M4, M5, and M6, respectively. The approximate positions of the slugs are shaded. The vertical axis is the distance off the bottom. The contour interval for temperature is 0.05°C, and the 6.18°C contour is also included. (e) The across-slope (negative to downslope, thick line) and along-slope (negative toward west, thin line) components of current measured by an Aanderaa current meter 2 m off the bottom at M6. The arrows show the pulses of downslope flow associated with the slugs. (f) Contours of acoustic scattering intensity (decibel) recorded by the ADCP at M6. The vertical axis is the distance off the bottom. The contour interval is 2.5 dB.

Table 1. Mean Properties of Slugs at the Vertical Arrays M5 and M6[a]

	M5	M6
Percentage	36	45
Duration, h	8.4 ± 7.1	11 ± 7.7
q, 10^{-2} m^2 s^{-1}	8.6 ± 4.4	32 ± 20
B_s, 10^{-2} m^3 s^{-2}	10 ± 18	36 ± 55
ΣB_s, m^3 s^{-2}	3.7	13.8
ΣB, m^3 s^{-2}	7.2	15.3

[a] The arrays are at 21 and 55 m depth and at about 400 and 900 m distance from the shore, respectively. The first row is the percentage of the total duration of slugs over the 38 day period of experiment II. The second row is the mean duration of the slugs. B_s and q are calculated using equations (1) and (2), respectively. ΣB_s is the total buoyancy flux carried by the slugs throughout the experiment. The last row is the total surface buoyancy flux integrated from the time the lake loses heat to the time the slug starts over the shelf to M5 (first column) and M6 (second column).

[18] Some mean properties of the slugs are summarized in Table 1. The increase in q with downslope distance (i.e., from M5 to M6) is consistent with the turbulent entrainment during the descent of a gravity current [*Ellison and Turner*, 1959] and the contribution of cold convective plumes from the surface [*Thorpe et al.*, 1999]. Ignoring the effects of diurnal stratification (see section 3.2), the convection timescale for these plumes to reach a thermocline depth D of O(100 m) is $(D^2/B)^{1/3}$, i.e., 1–2 hours. The slugs typically start 10 ± 7.0 hours after the onset of cooling, and therefore convection is probably well developed by the time slugs appear. The average volume of water carried by a slug across the 21 m depth contour at M5 is 5.3×10^3 m^3 m^{-1}, and this is about 1.9 times the volume of water in the wedge-shaped region from the shore to 21 m depth. In the shallows, slugs carry 50 ± 5% of the integrated surface buoyancy flux during cooling periods (compare the last two rows of Table 1). This agrees with the mean rate of change of buoyancy of the shallow waters, which was found to be equal to about 50% of B during the convective periods (for details, see section 3.2). The mean gradient Richardson number Ri is calculated during the passage of slugs at a level between 2 and 4 m above the bottom at M5 and 2 and 5 m at M6. At M5 it is found to be 0.19 ± 0.1, which is less than the critical value of 0.25, and the flow is dynamically unstable, whereas at M6 it increased to 1.1 ± 0.5.

[19] The time between the slugs' passing the arrays M5 and M6 and the known mooring horizontal separation allows estimates to be made of the mean front speed for each slug. The fronts of the slugs are found to move downslope with an average speed of $U = 5.2 \pm 3.5$ cm s^{-1}. Nondimensionalized front speeds of slugs, $U/b^{1/3}$, where b is the integrated surface buoyancy flux over the time period from one slug to the next, is shown in Figure 4a as a function of $\overline{d}/|L|$. Here L is the Monin-Obukov length and $\overline{d}$ is a mean shelf depth, i.e., the average depth to the "shelf break" where the bottom slope increases sharply (about 300 m from shore in Figures 2a–2b). During relatively calm periods, i.e., $\overline{d}/|L| > 1$, U is found to be equal to $(1.3 \pm 0.4)b^{1/3}$, and the ratio of the slug head speed to the speed of the following flow is $U/\overline{u} = 0.8 \pm 0.3$. Both values are close to those proposed by *Britter and Linden* [1980] for fronts of gravity currents, U_f. *Britter and Linden* [1980] find that the leading head of the gravity current grows as it moves downslope. The speed of the front, U_f, normalized by the cube root of the steady buoyancy flux in the gravity current per unit along slope length at the top of the slope B_o given by $U_f/(B_o)^{1/3} = 1.5 \pm 0.2$, almost independent of the slope angle β for $5° \leq \beta \leq 90°$. The following flow has a speed u of about $1.6U_f$ or $U_f/u \approx 0.63$.

3.1.3. Pulses

[20] The temperature data recorded by the bottom miniloggers during experiment I were analyzed to seek pulses of cold and plane temperature fronts moving down and along the slope with uniform propagation speed near the lateral bottom boundary. The four periods, A–D, selected for analysis are summarized in Table 2. The surface cooling during periods A, C, and D was interrupted by 4–5 hours of daytime warming, while the lake was losing heat throughout period B.

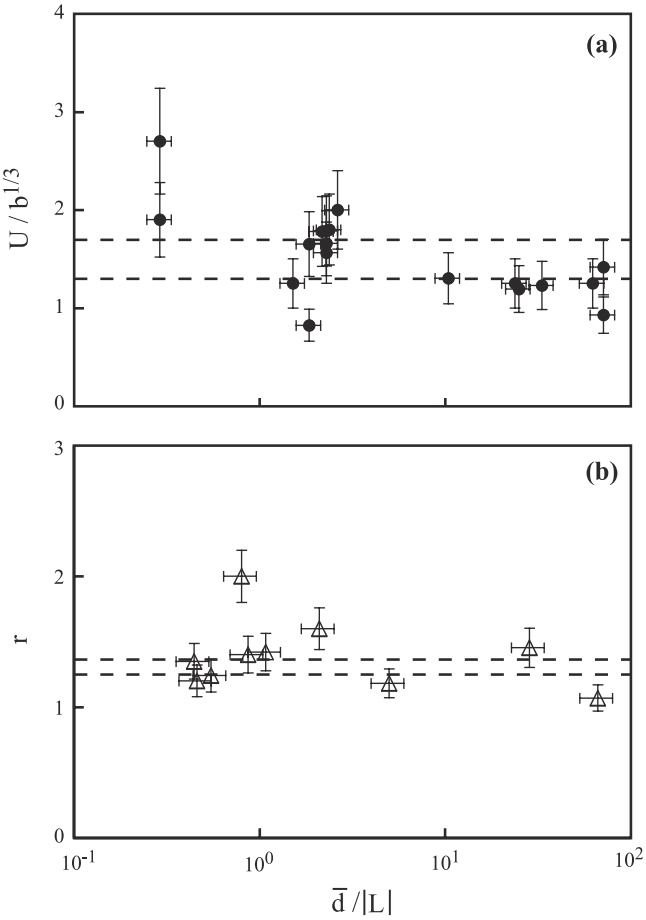


Figure 4. (a) Nondimensionalized downslope speeds of leading fronts of slug, $U/b^{1/3}$, as a function of $\overline{d}/|L|$. Here b is the integrated surface buoyancy flux over the time period from one slug to the next, $\overline{d} = 4$ m is the mean shelf depth, and U is the mean speed of the leading fronts of slugs observed during experiment II. For $\overline{d}/|L| > 1$, $U/b^{1/3}$ is found to be equal to 1.3 ± 0.4. The dashed lines show the range of normalized front speeds of gravity currents on an incline, 1.5 ± 0.2, given by *Britter and Linden* [1980]. (b) The ratio r of pulse speed to the mean flow in the slug as a function of $\overline{d}/|L|$. Here r is found to be equal to 1.38 ± 0.3 (see section 3.1.3). The dashed lines show the range reported for roll wave observations in the turbulent open channel near Grünnbach in Switzerland [*Cornish*, 1934].

Table 2. Periods of Experiment I Selected for Analysis[a]

Period	Date/Time (1998 / LT)	Length, hours	Percentage	$-L$, m	B, 10^{-8} m^2 s^{-3}
A	21 Nov. / 0000 22 Nov. / 0600	30	87	7.9 ± 2.0	4.5 ± 0.9
B	1 Dec. / 0000 4 Dec. / 0000	72	100	2.2 ± 1.5	2.5 ± 0.8
C	8 Dec. / 0000 11 Dec. / 0000	72	89	0.3 ± 0.2	2.3 ± 0.9
D[b]	20 Dec. / 1200 24 Dec. / 0000	84	89	4.2 ± 3.0	2.2 ± 1.5

[a] The third column is the record length, and the fourth column is the percentage of the cooling hours over the record length. L is the mean Monin-Obukov length, and B is the mean surface buoyancy flux averaged over the cooling hours of each period.

[b] Miniloggers at 5, 10, 17.4, and 23 m depth recorded until 15 December 1998.

[21] The analysis follows that used by *Thorpe and Lemmin* [1999] to describe internal waves and temperature fronts propagating between sensors along the sloping boundary of Lake Geneva. The downslope movement of large temperature time derivatives is detected as an ''event'' whenever the derivatives exceed a set threshold and can be followed reaching the center of the cross of the minilogger lines laid along and down the slope, satisfying the condition of passing at least three consecutive sensors in both lines. The threshold selected is the value limiting the 85 percentile in the histogram of temperature time derivatives at each sensor. Threshold values ranged from 6.7×10^{-5}°C s^{-1} to 2×10^{-4}°C s^{-1}. The irregular downslope separation of the miniloggers (see section 2.1 and Figure 1b) is carefully accounted for in the detection of uniform speed events. Features with propagation speeds <0.03 m s^{-1} were discarded and were not included in the analysis below because current measurements that are used for the verification become unreliable below this value. The relatively large time duration and propagation distances of events found in the analysis suggest that they correspond to features propagating as gravity currents and are not a consequence of chance time and space alignments of large temperature derivatives, which would have shorter time duration and smaller propagation distances (see Appendix A).

[22] During periods of steady surface cooling, estimates of the mean speed of pulse fronts are obtained by averaging the propagation speed of recognized events. Figure 4b shows the ratio r of the speed of pulses to that of the mean flow measured by the current meter at M2. Here r is found to be equal to 1.38 ± 0.3; the pulses move about 40% faster than the mean flow.

[23] Pulses are mostly detected first at depths between 2 and 25 m and can be followed downslope for a distance of 358 ± 90 m. Only 5% of the pulses cover a downslope distance of over 700 m throughout the line of miniloggers. Their average downslope speed is u_p = 6.5 ± 2.8 cm s^{-1}. They extend to a distance of 239 ± 40 m along the slope with an average speed of v_p = 8.0 ± 3.1 cm s^{-1}. Ninety percent of the events move cyclonically (i.e., with a positive component of speed to the west), consistent with a deviation of the gravity current by the Earth's rotation and in accord with laboratory studies [*Whitehead et al.*, 1990; *Lane-Serff and Baines*, 1998, 2000]. However, it appears unlikely that rotational control will be complete or that the flow will be in quasi-geostrophic balance since the duration of the slugs is much less than the local inertial period, 17.4 hours. The speed histograms of the detected pulses are shown in Figure 5 for (a) downslope and (b) alongslope propagation. For all the analyzed periods the histograms show peaks at downslope and alongslope flow speeds of about u_p = 5 cm s^{-1} and v_p = 7.5 cm s^{-1}, respectively. The orientation of the front of pulses is calculated to be 56° across isobaths.

[24] A 36 hour section of two nocturnal cooling cycles during period B is shown in Figure 6. The surface buoyancy flux B is positive (lake losing heat) throughout the period (Figure 6a). The isotherms derived from M1 (Figure 6b) show a relatively cold layer of 2–5 m thickness associated with the passage of the pulses. They persist at a given location for 1–3 hours. The ratio of average temperature variations in the pulses to the average temperature difference of temperature in the slug and the overlying fluid is 0.45 ± 0.09. The location of the vertical array, M1, is marked by a dashed line in Figure 6c, which shows the isotherms with respect to downslope distance. The pulses can be followed to 800 m downslope from the shore. The upslope component of the bottom current recorded 2 m off the bottom at M2 (Figure 6d) shows downslope (negative) pulses as a consequence of the draining of cold water. The ratio of the size of velocity variations in the pulses, u', to the mean flow is found to be $u'/\overline{u} = 0.32 \pm 0.05$. The pulses can be followed through the array of miniloggers laid along the slope (Figure 6e). The detected events with downslope and alongslope propagation are shown as lines in Figures 6c and 6e, respectively. Different slopes of the lines correspond to different speeds. The distance in Figure 6c is downslope, while that in Figure 6e is toward the west, along the slope.

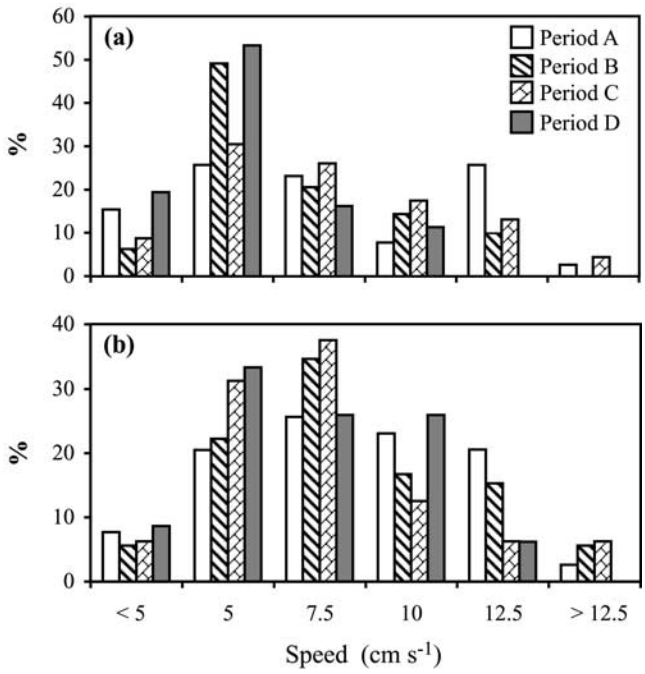


Figure 5. The speed histograms of the detected pulses moving (a) downslope and (b) cyclonically with uniform speed. The periods are summarized in Table 2. The labels in Figure 5b are same as in Figure 5a. A total of 182 events were detected.

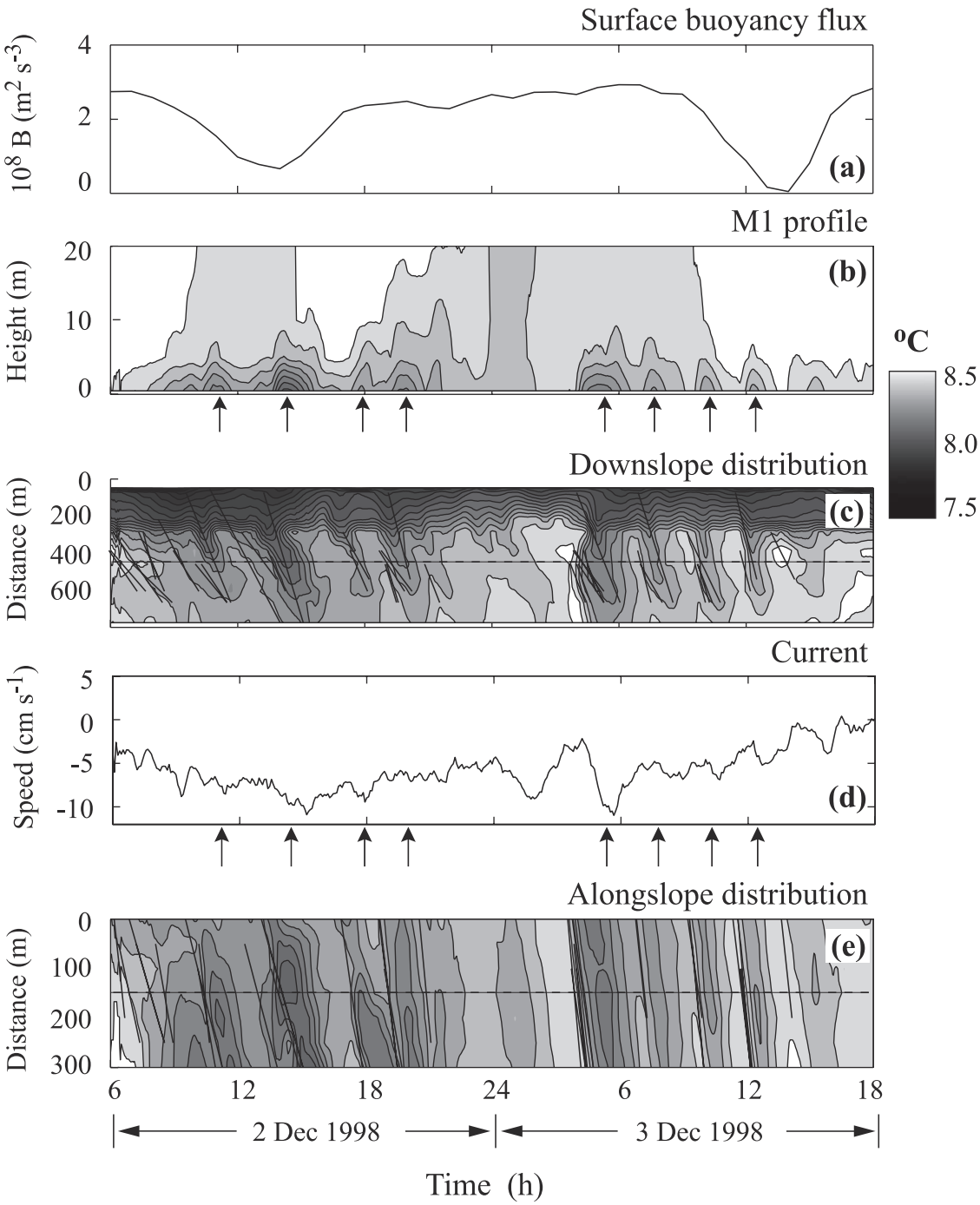


Figure 6. Pulses of cold water observed during the 36 hour section of period B of experiment I. The mean Monin-Obukov length scale L is −2.2 m. The isotherms are half hourly smoothed, and the contours are in degrees Celsius and are drawn at 0.02°C intervals. (a) Hourly averaged values of the surface buoyancy flux B. (b) Contours recorded by vertical thermistor array at M1. The vertical axis is the height above the bottom. The arrows mark the pulses of cold water. (c) Isotherms derived from the time series of temperature recorded by miniloggers laid at the bottom across the slope. The vertical axis is downslope distance from shore. The lines show the cold temperature front events propagating downslope. The dashed line marks the location of vertical array M1. (d) The upslope (negative to downslope) component of current measured by an Aanderaa current meter at 2 m off the bottom at M2. The arrows are same as in Figure 6b. (e) Isotherms derived from the time series of temperature recorded by miniloggers laid at the bottom along the slope. The vertical axis is distance toward west. The detected events are shown as lines. The dashed line is same as in Figure 6c.

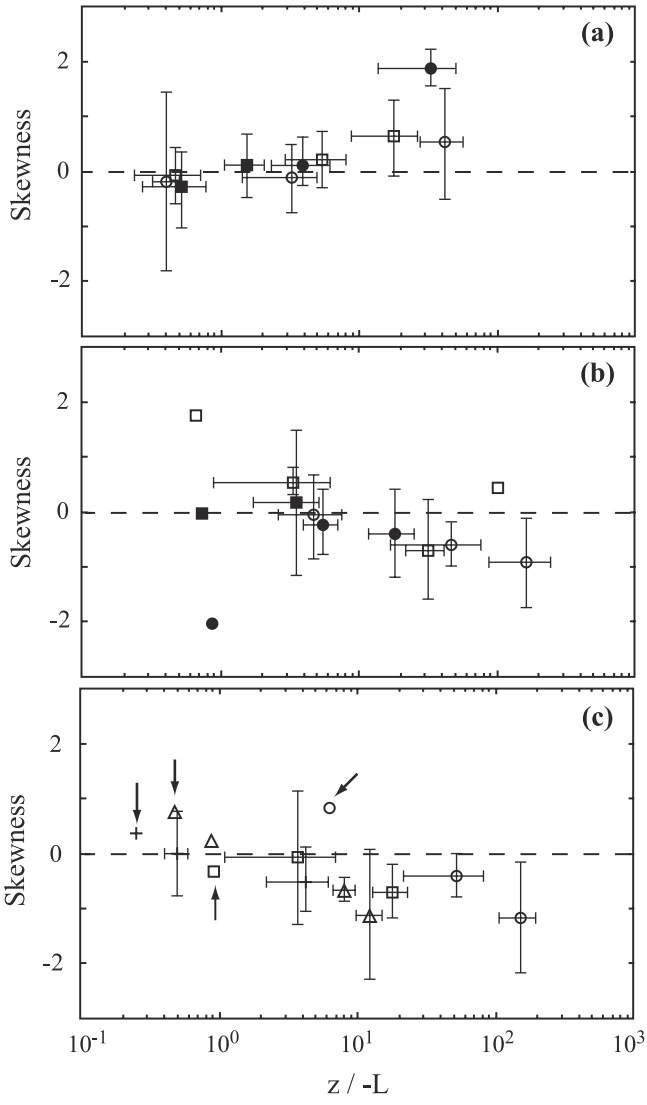


Figure 7. Skewness of temperature time derivatives, S, as a function of $z/-L$ measured at fixed positions. Here z is the sensor depth, and L is the Monin-Obukov length. S values are averaged in each decade of $z/-L$. The error bars show the standard deviations over averaged values. When there is none, it indicates that there is one value of S in that decade. (a) Values derived from the top sensors of moorings M4 (solid squares, northeasterly winds; open squares, southwesterly winds) and M5 (solid circles, northeasterly winds; open circles, southwesterly winds) during cooling periods of experiment II. (b) Values derived from the bottom sensors of moorings M4 (solid squares, northeasterly winds; open squares southwesterly winds) and M5 (solid circles, northeasterly winds; open circles, southwesterly winds) during cooling periods of experiment II. (c) Values derived from the miniloggers laid across slope at the bottom during period A (plus) B (open squares), C (open circles), and D (triangles) of experiment I. The arrows mark the near-surface minilogger 2 m below the surface at 4 m depth for each period.

Each pulse of cold water is associated with several front events, suggesting fronts and pulses may decelerate rather than have the assumed uniform downslope flow.

3.1.4. Skewness of temperature derivatives

[25] Measurements made during convectively unstable conditions in the atmospheric boundary layer [*Phong-Anant et al.*, 1980] and in the upper ocean boundary layer [*Soloviev*, 1990; *Thorpe et al.*, 1991] show evidence of temperature ''fronts'' leading to a skewed distribution of temperature time derivatives. Similar fronts or temperature ramps are found in stable heating conditions in the atmospheric boundary layer [*Antonia et al.*, 1979], lakes [*Thorpe and Hall*, 1980], and the ocean [*Thorpe*, 1985] and are believed to be evidence of large coherent structures.

[26] The distribution of the temperature time derivatives on the sloping sides of lakes or oceans also has an asymmetry due to the ebb and flow of internal waves. A periodic change in the sign of skewness of temperature derivatives, S, measured by moored sensors and associated with the on-slope and off-slope flow of internal waves at Porcupine Bank has been reported [*Thorpe et al.*, 1991]. The mean value of $|S|$ was 0.35 with a maximum of about 0.8. A small negative mean skewness of 0.05 has been found on the ''internal surf zone'' of Lake Geneva where internal waves interact with the sloping boundary [*Thorpe and Lemmin*, 1999].

[27] Values of S as a function of $z/-L$, where z is the depth of the sensor and L is the Monin-Obukov length, are calculated and shown in Figure 7 for the near-surface (Figure 7a and the points marked by arrows in Figure 7c) and the near-slope regions (Figures 7b–7c). The temperature recorded by the top and the bottom sensors of the moorings M4 (circles) and M5 (squares), during the periods when the lake is losing heat, is divided into 6 hour segments corresponding to 144 data values that have been used to calculate S in Figures 7a–7b. The top sensors are 0.8 and 6 m below the surface, and the bottom sensors are 0.5 and 1.2 m above the bottom. Figure 7c is obtained using the temperature data recorded by the miniloggers laid across the slope during periods A–D of experiment I. The sensors are 0.5 m off the bottom. For each period, there is one sensor near the surface, which is indicated by an arrow.

[28] In well-developed steady conditions, free convection (independent of mechanical mixing at the water surface) is established for $z/-L \gg 1$ [*Turner*, 1973]. Wind stirring is dominant for $z/-L < 1$. In order to identify the effect of wind direction on S, periods with NE (solid symbols) and SW (open symbols) winds are separated in Figures 7a and 7b. No clear trend with the wind direction is apparent for $z/-L < 1$.

[29] When the convective conditions are independent of wind forcing, i.e., $z/-L \gg 1$, there is a trend toward positive S near the surface in the shallows (Figure 7a) as a consequence of inflowing warm fronts. In contrast, near the sloping bottom it is toward negative S (Figures 7b–7c) persisting to depths of 60 m (note that the deepest bottom sensor in experiment I is laid at 56 m depth). The trends in Figures 7b–7c are comparable. The skewness values obtained from the near-surface sensor, marked by arrows, are expected to be influenced by the wind during periods A, B, and D, while period C is under free-convection con-

ditions. Positive values of S are found near the surface during periods A, C, and D. This agrees with the trend in Figure 7a.

[30] Here we suggest that during winter the skewness of the temperature time derivatives, S, measured at fixed positions in the lake may be influenced by the following mechanisms: (1) convection near the surface (as in the atmosphere and the ocean), producing negative S (or positive S in stable heating); (2) the convective circulation near the surface in shallow water, induced by the repetitive cascading of cold water from the shelf and the inflow of warmer offshore water, forming warm temperature fronts leading to positive S; and (c) the draining cold water down the bottom slope that supplies the cascade involves cold temperature fronts, leading to negative S. Observations are consistent with the three identified mechanisms. They imply that warm water near the lake surface is moving from the open waters onto the shelf region, replacing the volume discharged from this area by the cascade. This circulation pattern confirms the results of *Sturman et al.* [1999].

3.2. Mean Diurnal Cycle

[31] The mean cycle of diurnal heating and nocturnal cooling is illustrated in Figures 8–9 by averaging 5 hours before to 31 hours after the mean time of warming over several periods of similar diurnal forcing in which there is diurnal convection with $B > 1.8 \times 10^{-8}$ m^2 s^{-3}. The behavior of the slugs on the slope can be seen from mean isotherms derived from miniloggers laid at the bottom during experiment I. Figure 8a is the average surface buoyancy flux over four 36 hour periods. Figure 8b is the temperature contours obtained from sensors deployed down the slope. Distance is the downslope distance from shore. About 7 hours after the local time, 1500 LT, when cooling commences, the draining cold water reaches the 30 m isobath ($\sim$500 m from shore), and two sensors following similar downslope movements can be seen 11 and 15 hours after the start of cooling (events marked by arrows in Figure 8b). They persist to the depth contour of 56 m, about 800 m distance from the shore, and can be followed passing through the vertical arrays at 30 (M1, Figure 8c) and 56 m (M2, Figure 8d) depth. The isotherms in Figure 8e are calculated from the miniloggers laid along the slope, and the distance is toward west. The downslope movement of cold water is associated with a westward transport along the slope. This suggests that the front of cold water is not parallel to the shelf break and that the shelf is not draining in a two-dimensional manner. This is possibly a consequence of the spatial irregularities on the shelf and will be discussed later.

[32] Figure 9a shows the surface buoyancy flux averaged over 7 days in experiment II, and Figures 9b and 9c show the mean isotherm depth versus time contours at M4 (above 5 m depth contour) and M6 (above 56 m depth contour), respectively. The 24 hour diurnal cycle is clearly seen. During 5 hours of daytime warming beginning at time t = 1000 LT the temperature of the water column in the shallow water at 5 m depth (Figure 9b) gradually increases, and a thermocline forms at middepth. Cooling begins at t = 1500 LT of day 1. The shallow water thermocline becomes weaker ,and by t = 1800 LT, about 3 hours after the cooling starts, the water column is again uniform in temperature (see the arrows under Figure 9b). This is about 6 times the convective timescale $(D^2/B)^{1/3}$ of 0.5 hours, with D = 5 m and $B = 2 \times 10^{-8}$ m^2 s^{-3}; convection takes longer to mix the stratified water column with its diurnal thermocline. The times of maximum temperature are marked by dots. Heating at 56 m depth does not end until t = 2100 LT, well after surface heating has ended, indicating a mixing time of about 6 hours to 56 m. Assuming that the only heat transfer is vertical diffusion, this leads to an effective diffusion coefficient of about $56^2/(6 \times 3600) \approx 0.15$ m^2 s^{-1}. As the heat loss from the surface continues, a slug of cold water appears near the bottom at 56 m, at t = 0300 LT of day 2, marked by enhanced temperature time derivative. The mean rate of change of buoyancy, db_{5m}/dt, of the water column at 5 m averaged over the selected seven periods is also shown in Figure 9a (thin line). During periods of warming, db_{5m}/dt is approximately balanced by the surface buoyancy flux B. During convective conditions it only averages about 50% of B. This agrees with estimates based on the buoyancy flux in the downslope flowing water (see section 3.1) and implies that the buoyancy carried by the slugs is replaced by positive buoyancy circulated into the shallow waters around the side of the lake from deeper water (an onshore transfer of relatively warm water), providing further evidence of convective circulation.

[33] The velocity structure associated with the mean diurnal cycle of the cascade shows a layer close to the bottom moving downslope. Its thickness increases with time and is reduced at t = 1200 LT responding to surface warming. The mean vertical profile of upslope component of the speed recorded at M6 shows a downslope moving layer of thickness $h \sim 20$ m [*Fer*, 2001]. Although the flow cannot be measured by the ADCP closer than 6 m from the surface, it appears that vertically integrated upslope and downslope flow are in approximate balance with no net flux [*Fer*, 2001].

[34] The currents on the sides of the lake are, however, strongly influenced by the surface buoyancy flux B. The bottom current at 21 m depth responds to diurnal variations in B with approximately no phase difference, while at 56 m depth it has a time lag of 6 hours. The downslope components of bottom currents recorded at M5 and M6 are found to be coherent around diurnal periods with a phase difference of about 50° during convective conditions. The mean currents at the bottom are downslope and cyclonic, anticlockwise here, for both experiment periods.

4. Discussion

4.1. Mean Discharge of Cold Water From Shallows

[35] The net discharge from the shelf region around the whole lake can be estimated from the surface buoyancy flux B. We can generalize the properties of the slugs obtained in the vicinity of Buchillon where there is a well-defined shelf reaching some 400 m from the shore, extending to lake scale. Suppose that the shallow water regions are periodically flushed at time intervals τ determined, for example, by the movement of warm fronts entering from deep water and the reflection from shore of a wave into the new stratified waters. The speed of waves or gravity currents on the shelf is proportional to $(g'\bar{d})^{1/2}$, where $g' = g\alpha\Delta\theta$ is the reduced acceleration of gravity and $\bar{d}$ is the mean shelf depth. Here α is the coefficient of expansion and $\Delta\theta$ is the temperature

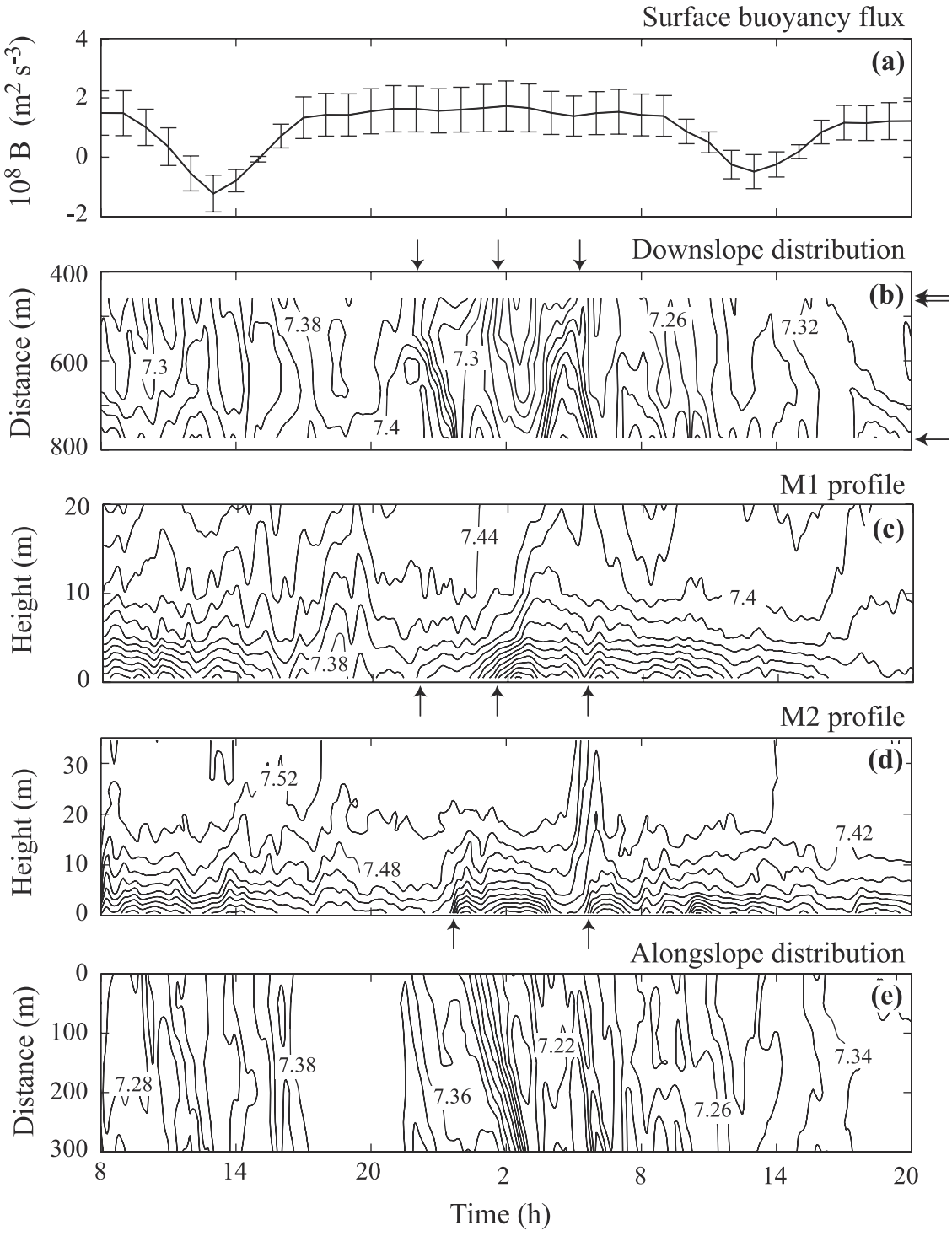


Figure 8. Mean cycle of diurnal cascading obtained by averaging four periods in which there is diurnal convection with $B > 1.8 \times 10^{-8}$ m^2 s^{-3} during experiment I. The contours are in degrees Celsius with 0.02°C intervals. Time is local time. (a) Mean surface buoyancy flux B. The error bars represent the standard deviation over four periods. (b) Isotherms derived from downslope miniloggers. The vertical axis is the downslope distance measured from the shore. The draining of cold water is shown by arrows at the top. (c) and (d) Temperature contours, height above the bottom versus time, obtained from vertical arrays at 30 (M1) and 56 m (M2), respectively. The positions of the arrays are shown by the arrows on the right of Figure 8b. (e) The isotherms calculated from the 300 m long array of miniloggers laid along the slope. The distance is toward the west.

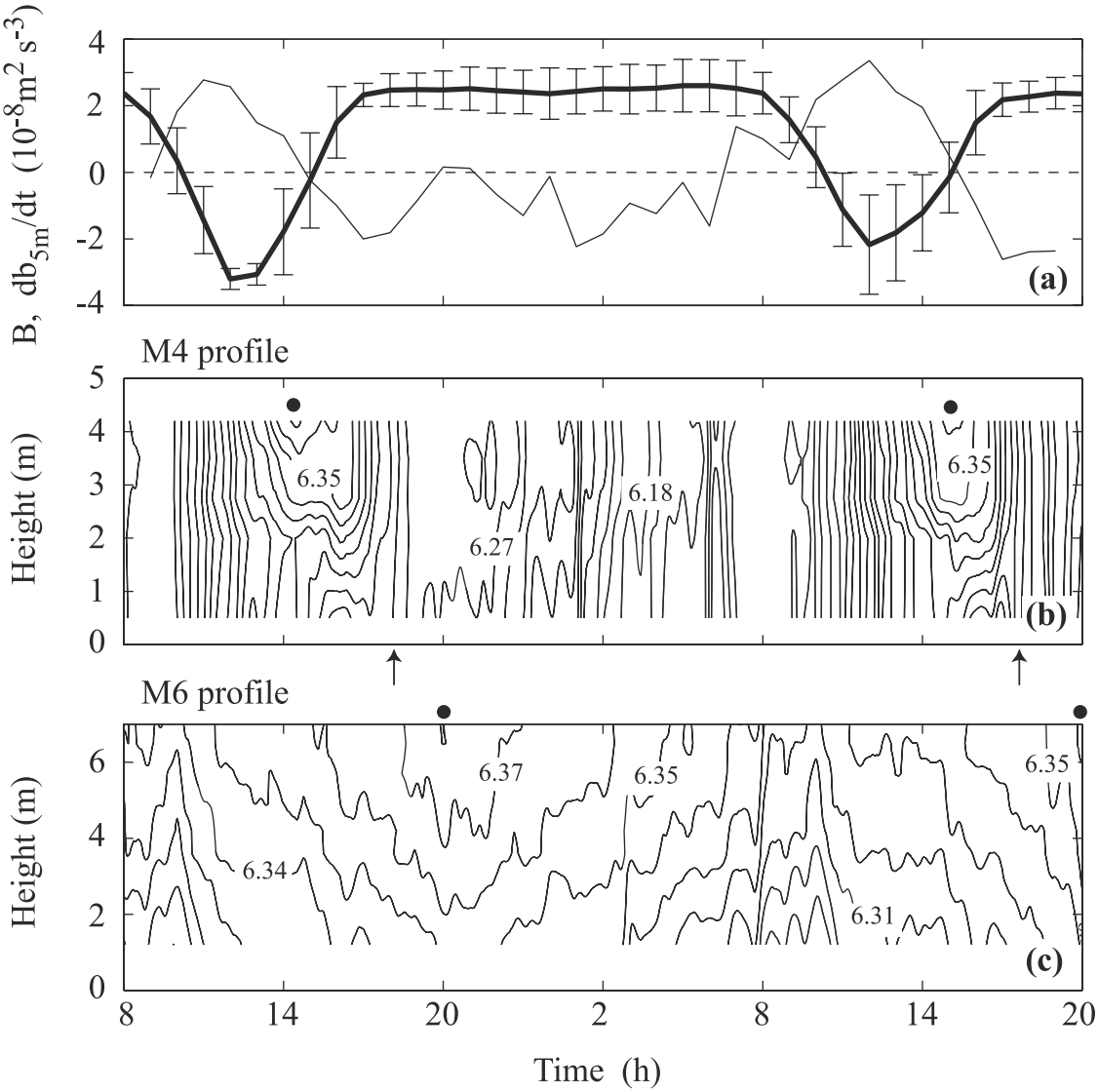


Figure 9. Mean diurnal cycle obtained from seven similar periods of strong diurnal forcing during experiment II. The contours are in degrees Celsius with 0.01°C intervals. Time is local time. (a) Mean surface buoyancy flux B (thick line) and the mean rate of change of buoyancy, db_{5m}/dt, of the water column at 5 m depth (thin line). The error bars represent the standard deviation over seven periods. (b) and (c) Isotherms, height versus time, derived from vertical arrays at M4 (5 m) and M6 (55 m). The arrows in Figure 9b show the time the water column is mixed after the onset of cooling. The dots in Figures 9b and 9c mark the times of maximum temperature.

difference between either the surface and bottom water in the shallows for waves or the shallow and deep water for gravity current fronts. A timescale for the flushing of shelf waters, τ, is then

$$\tau = l \Big/ \sqrt{g'\overline{d}}, \tag{3}$$

where l is shelf width. The effects of rotation are assumed to be negligible. If we assume that $\Delta\theta$ is determined by the heat flux during the period τ between shelf flushing events, then

$$g' \sim \left(B\tau/\overline{d}\right), \tag{4}$$

where B is the surface buoyancy flux. Using equations (3)–(4) the flushing timescale is

$$\tau = kl^{2/3}B^{-1/3}, \tag{5}$$

independent of $\overline{d}$, where k is a constant. The volume of cold water, V, carried from the shallow region per unit width of the lake over a cooling time period of T_c depends on how many times, T_c/τ, the shelf is flushed:

$$V = V_s T_c/\tau, \tag{6}$$

where $V_s = \overline{d}\, l$ is the volume of the shelf. Typical values of T_c = 18 hours, l = 400 m, $V = 1.9V_s$ (section 3.1.2), and

$B = 2.5 \times 10^{-8}$ m^2 s^{-3} obtained for Buchillon yield a factor k of 1.8 and a local flushing time τ of 9.3 hours. Fronts in Figures 8 and 9 suggest that pulses are not random in time, which supports our assumption of "periodic discharge" rather than random events. On the other hand, the time interval between pulses is about 3 hours (see arrows in Figures 6 and 8), which is less than τ, and the shelf water appears not to flush completely (see Figure 6c). This suggests that τ is a fictious time, equivalent to effective total flushing by more frequent pulses, each of which removes about one third of the shelf water. The pulse frequency is not determined by intervals between "complete" discharge from the shelf.

[36] The total discharge of cold water spilling down per unit width of the sides of the lake is

$$Q \sim (T_c/T)\overline{d}l^{1/3}B^{1/3}, \tag{7}$$

where T is the total time and T_c/T is 0.36. This increases with, but is not very sensitive to, both B and l. Introducing typical values of $B = 10^{-8}$ m^2 s^{-3}, $\overline{d} = 4$ m, and $l = 100$ m (possibly an underestimate) and integrating around the 100 km circumference of the depth contours of $\overline{d}$, this yields a total discharge of 2300 m^3 s^{-1}, which is an order of magnitude estimate and is about 11.5 times the total river inflow of 200 m^3 s^{-1} during winter.

[37] The analysis given here is valid if there is a well-defined shelf and applies to diurnal heating, when $\tau < 24$ hours. For the oceanic continental shelf where l is typically about 100 km the downslope flow, the discharge, and the circulation will be affected by the Earth's rotation.

4.2. Nature of the Pulsing Flow

[38] The pulses travel faster than the mean flow in the gravity current (Figure 4b). The ratio of the speed of pulse fronts to the mean flow is $r = 1.38 \pm 0.3$. They are therefore not a consequence of Kelvin-Helmholtz, Holmboe instability, or the waves observed by *Farmer and Armi* [1999] in the downslope flow behind the sill at Knight Inlet, all of which have speeds within the range of the mean flow. Fronts propagating faster than the mean flow in a periodic manner are characteristic of roll waves in open channel flows, when the flow is supercritical [*Dressler*, 1949]. The internal Froude number associated with the gravity-driven flow in a slug of mean speed of $U = 5$ cm s^{-1} and a thickness of $h = 5$ m is $Fr' = U^2/g'h \sim 20$ for a temperature difference $\Delta\theta$ of 0.05 K ($g' = g\alpha\Delta\theta$ is the reduced gravity, and as before, α is the coefficient of expansion, 4.6×10^{-5}°C^{-1} at 7°C). The Reynolds number $Re = Uh/\nu$ (ν is the kinematic viscosity $\sim 10^{-6}$ m^2 s^{-1}) is about 3×10^5, and the mean slope of the observation site is about 4.6° (section 2). These values are comparable to those of $Fr = 18.6$, $Re = 1.5 \times 10^5$, and $r = 1.3 \pm 0.06$ (dashed lines in Figure 4b) reported for roll wave observations in the turbulent open channel of Grünnbach having a mean slope of 5.5° [*Cornish*, 1934] and suggest a dynamical similarity. The necessary condition for roll waves to exist in open channel flows at high Re is $Fr > 4$ [*Dressler*, 1949]. Profiles of salinity and temperature from the center of the Hatteras Abyssal Plain led *Armi* [1977] to suggest that roll waves may be important for bottom boundary layers since Fr' can be relatively high. At relatively low Re, pulsing flows are also found in turbidity currents [*Hay*, 1987], in layers of flowing grains [*Prasad et al.*, 2000], and in laboratory studies of gravity flows on inclines [*Alavian*, 1986; *Whitehead et al.*, 1990; *Zatsepin et al.*, 1996; *Lane-Serff and Baines*, 1998].

[39] Consider the flow of a gravity current down a uniform slope beneath a deep less dense quiescent layer with no rotation, negligible entrainment, and no convective plumes. The conservation of flux and density in the current implies

$$\frac{\partial h}{\partial t} + \frac{\partial}{\partial x}(hu) = 0 \tag{8}$$

$$\frac{\partial \rho}{\partial t} + u\frac{\partial \rho}{\partial x} = 0, \tag{9}$$

and the momentum equation is

$$\frac{\partial u}{\partial t} + u\frac{\partial u}{\partial x} = \frac{g(\rho - \rho_0)}{\rho_0}\left(\sin\beta - \frac{\partial h}{\partial x}\right) - \frac{C_D u^2}{h}, \tag{10}$$

where h is the thickness of the gravity current, u is the mean speed of the flow in the current, β is the inclination angle, and C_D is a drag coefficient including the effects of both the bottom and the interface between the dense layer of density ρ and the overlying water of density ρ_o. The representation of drag is identical to the Chézy formulation used in open channel flows. Here it represents the stress of both the bottom and the interface at the top of the gravity current. Equations (8) and (10) are identical to those used by *Needham and Merkin* [1984] for roll waves in open channel flows, although in their analysis, ρ remains constant. Here, because there is no mixing with the overlying layer, density fluctuations are advected according to equation (9).

[40] The steady state balance gives the mean downslope flow

$$\overline{u} = \left[\frac{g(\overline{\rho} - \rho_0)}{\rho_0}\frac{\overline{h}\sin\beta}{C_D}\right]^{1/2}, \tag{11}$$

where $\overline{\rho}$ is the mean density of the gravity current. This is in accord with observations (see section 1). Following Needham and Merkin, perturbing the equations and linearizing with respect to the mean gravity current values $\overline{u}$, thickness $\overline{h}$, and density $\overline{\rho}$, so that $u = \overline{u} + u'$, $h = \overline{h} + h'$, and $\rho = \overline{\rho} + \rho'$ gives

$$\left(\frac{\partial}{\partial t} + \overline{u}\frac{\partial}{\partial x}\right)h' = -\overline{h}\frac{\partial u'}{\partial x}, \tag{12}$$

$$\left(\frac{\partial}{\partial t} + \overline{u}\frac{\partial}{\partial x}\right)\rho' = 0, \tag{13}$$

$$\frac{\partial u'}{\partial t} + \overline{u}\frac{\partial u'}{\partial x} = \frac{g\rho'}{\rho_0}\sin\beta - \frac{g(\overline{\rho} - \rho_0)}{\rho_0}\frac{\partial h'}{\partial x} - \frac{C_D\overline{u}^2}{\overline{h}}\left(\frac{2u'}{\overline{u}} - \frac{h'}{\overline{h}}\right). \tag{14}$$

The first term on the right of equation (14) is not found in the roll wave theory in open channel flows. In the classical roll wave theory, h' is eliminated by taking $(\partial/\partial t + \overline{u}\partial/\partial x)$ of

equation (14) and substituting from (12) for $(\partial/\partial t + \overline{u}\partial/\partial x)h'$. Here, taking of $(\partial/\partial t + \overline{u}\partial/\partial x)$equation (10) and using equation (13) results in an identical equation since $(\partial/\partial t + \overline{u}\partial/\partial x)\rho' = 0$. Linear solutions of free-surface and interfacial waves are therefore identical, provided that the acceleration of gravity, g, is replaced by the reduced acceleration of gravity, $g' = g(\overline{\rho} - \rho_0)/\rho_0$. Hence the necessary condition for interfacial roll waves to exist is $Fr' = \overline{u}^2/(g'\overline{h}) > 4$, where Fr' is the internal Froude number, or using equation (11), $\sin\beta/C_D > 4$. Our measurements (section 1) suggest that $C_D = (4 \pm 0.7) \times 10^{-3}$, and this leads to $\sin\beta/C_D$ of about 20 on the $4.7 \pm 0.6°$ slope, well above critical. *Needham and Merkin* [1984] show that the phase speed of waves, c, at the exchange of stabilities (zero growth rate) is (3/2) $\bar{u}$. This speed can be predicted by the application of the continuity equation in a coordinate system moving with c. If the speed and the thickness of the gravity current downstream and upstream of the pulse front are u_1, h_1, u_2, and h_2, respectively, the equation of continuity can be written as

$$(u_2 - c)h_2 = (u_1 - c)h_1. \tag{15}$$

[41] Supposing that the quasi-steady speeds u_1 and u_2 on the two sides of the front can be obtained by using equation (11) with corresponding values of h_1 and h_2, the ratio of the phase speed to the mean flow, $c/\overline{u}$, can be obtained as

$$\frac{c}{\overline{u}} = \frac{2\left(h_2^{3/2} - h_1^{3/2}\right)}{(h_2 - h_1)\left(h_1^{1/2} + h_2^{1/2}\right)}, \tag{16}$$

where the mean flow is $\overline{u} = (u_1 + u_2)/2$. Introducing $h_2^{1/2} = h_1^{1/2}(1 + h')$, with $h' \ll 1$, and only retaining the terms of $O(h')$, equation (16) yields $c/\overline{u} = 1.5$, compared to our observed value of $r = c/\overline{u} = 1.38 \pm 0.3$ (see Figure 4b). In reality the nonlinear terms neglected here and in equations (12), (13), and (14) may be significant since typically $u'/\overline{u} = 0.32 \pm 0.05$ and $\rho'/(\overline{\rho} - \rho_0) = 0.45 \pm 0.09$ (see section 3.1.3), and further study of this is merited, as well as of entrainment.

4.3. Cyclonic Motion of Pulses

[42] The irregularities in the shelf width (see, e.g., 5 m depth contours in Figure 1b) may lead to differential cascading of cold water, consequently causing the front of the gravity current to incline across the local isobaths. The orientation of the front pulses are calculated to be 56° across the isobaths, using the mean downslope and alongslope speeds of the cold temperature front events presented in section 3.1.3. This suggests that relatively larger shelf region some 400 m to the east of the thermistor line laid on the bottom may act like a source, feeding the cascade. While the net diurnal southward downslope flow in the gravity current is approximately equal to the net northward flow toward shallow water, the flow is not balanced at all times during the diurnal cycle. This suggests that alongslope flow is important.

[43] When the current flows along constant depth contours, the Ekman transport in the bottom boundary layer will tend to move water up or down the slope, in a rotating system. In Buchillon the flow is downwelling favorable with the mean current toward the west. The classical Ekman layer theory shows that the boundary layer thickness is $(2K_z/f)^{1/2}$ and that the corresponding transverse transport is $(K_z/2f)^{1/2}v$, where K_z is turbulent eddy viscosity, f is the Coriolis parameter, and v is the alongslope velocity above the boundary layer [*Pedlosky*, 1979]. For typical values of $K_z = O(10^{-4})$ m^2 s^{-1} near the slope [*Fer et al.*, 2002] and $v = 0.05$ m s^{-1} the boundary layer thickness is about 1.4 m, and the downslope Ekman transport is found to be 0.035 m^2 s^{-1} per unit width of the lake. The observed downslope transport driven by the cascade has a downslope speed $U = 0.05$ m s^{-1} and a thickness $h = 10$ m and is 0.5 m^2 s^{-1} per unit width of the lake. This is an order of magnitude greater than the downslope Ekman transport and suggests that the observed downslope flow is not only an effect of rotation. The alongslope flow will therefore amplify or aid the downslope gravity flow [*Condie and Rhines*, 1994], but the Ekman flow contribution to the net downslope flow is relatively small.

5. Conclusions

[44] We have observed a diurnal cycle in which the stabilizing surface buoyancy flux of daytime heating is followed by nocturnal cooling when the convective processes take place. Following the onset of cooling, turbulent mixing associated with the unstable surface layers of shallow waters starts to erode the stable temperature structure established during heating. This process mixes the water column in the shallow shelf region, and the cold water, relatively denser than that in open waters, starts to descend down the slope as a cold gravity current. This cascade of cold water over the sides of Lake Geneva is periodic on at least two timescales: one associated with slugs lasting 8 hours on the average and another associated with pulses of colder water traveling downslope through the slug gravity current in a manner similar to roll waves in a steep open channel flow.

[45] The average volume of cold water drained by the cascade amounts to about 1.9 times the volume of water on the shelf between shore and 21 m depth. Integrated around the lake, it is 11.5 times the mean river inflow during winter. It induces a convective circulation with about 50% of the heat lost in the shallows being supplied by inflow from deep water replacing that lost in the cascade.

[46] The observations demonstrate that the draining of cold waters during winter is an effective mechanism for flushing the shallow, nearshore regions. An enhanced acoustic scattering in high downslope flows suggests the cascade is also sometimes fast enough to erode and transport suspended sediment together with their dissolved components, oxygen, and pollutants into deeper water. The chemical, geological, and biological effects of the winter cascade of cold water from the lateral sides of lakes and from the continental shelves surrounding the oceans deserves further study.

Appendix A: On the "False Detection" of Temperature Front Events

[47] Events accepted as moving fronts by the algorithm explained in section 3.2 may include a sequence of ran-

domly occurring high gradients at neighboring sensors that have relative time delays that would indicate, falsely, that they are an event moving past sensors at uniform propagation speed. The probability of such false events can be estimated using a model data set following a procedure similar to that of *Thorpe and Lemmin* [1999]. A data set is simulated in which the large negative temperature gradients are distributed randomly but have the same mean duration and time separation as the measured data set at each sensor. Here duration is the time when the large gradients exceeding the set threshold persisted until they are interrupted by a low gradient, and the separation is the time between the last recognized high gradient to the present one. The overall mean time separation averaged over four periods (Table 2) is 14.9 ± 1.5 min for the alongslope line of sensors and 25.8 ± 6 min for the downslope one. The average duration of high gradients is 6.4 ± 0.5 and 5.9 ± 0.3 min for alongslope and downslope sensors, respectively. In total, 182 events are detected during 294 hours of analysis periods of A–D, which yields about 15 events per diurnal cycle. On the other hand, only 62 features were detected as events using the model data set.

[48] The frequency distributions of the duration of the detected events (here duration is the total time an event can be followed with a uniform speed) for the model data set and the measured one are compared in Figure A1. The model predicts a greater portion of events with smaller lifetimes for both downslope (Figure A1a) and alongslope (Figure A1b) sensors. Figure A2 shows the histograms of the length of detected events. More significantly, a greater proportion of events persisting to longer distances, reaching 700 m for downslope sensors and covering the total range of 300 m for alongslope ones, is observed than predicted by the model data set. The longer time duration and greater proportion distances of events found in the analysis suggest they correspond to features propagating as gravity currents and are not a consequence of chance time-space alignment of large gradients.

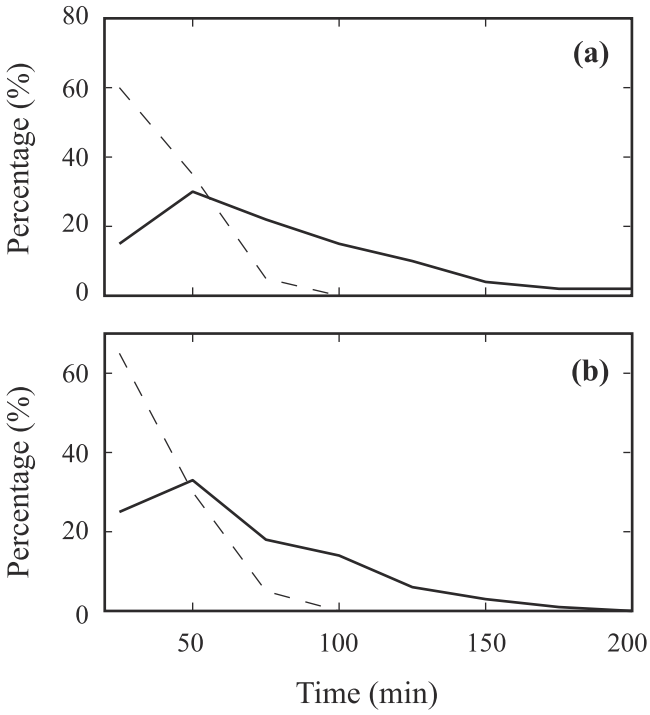


Figure A1. Frequency distributions of the duration of the events traveling (a) downslope and (b) to the west (cyclonically). The solid line is the average distribution obtained over four analysis periods (Table 2). The dashed line is the distribution obtained for the model data set having same number of high-temperature gradients at each sensor with the same time duration and separation as the measured one but at random times.

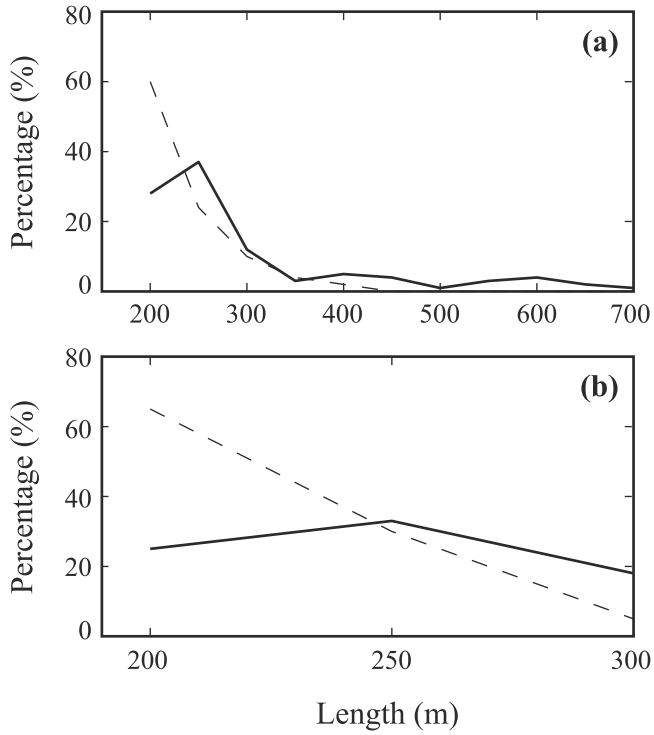


Figure A2. Frequency distributions of the length of the events traveling (a) downslope and (b) to the west (cyclonically). The solid line is the average distribution obtained over four analysis periods (Table 2). The dashed line is the distribution obtained for the model data set having same number of high-temperature gradients at each sensor with the same time duration and separation as the measured one but at random times.

[49] **Acknowledgments.** We are grateful for the financial support that was provided by the Swiss National Science Foundation, grant 20-49502.96, for this study. The constructive comments of the anonymous reviewers and their assistance in evaluating the paper are gratefully acknowledged.

References

Alavian, V., Behavior of density currents on an incline, *J. Hydrau. Eng.*, *112*, 27–42, 1986.

Antonia, R. A., A. J. Chambers, C. A. Friehe, and C. W. V. Atta, Temperature ramps in the atmospheric surface layer, *J. Atmos. Sci.*, *36*, 99–108, 1979.

Armi, L., The dynamics of the bottom boundary layer of the deep ocean, in *Bottom Turbulence, 8th International Liège Colloquium on Ocean Hydrodynamics*, edited by C. J. J. Nihoul, pp. 153–164, Elsevier Sci., New York, 1977.

Baines, P. G., S. Condie, Observations and modelling of Antarctic downslope flows: A review, in *Ocean, Ice, and Atmosphere: Interactions at the Antarctic Continental Margin Antarct. Res. Ser.*, vol. 75, edited by S. Jacobs and R. Weiss, pp. 29–49, AGU, Washington, D.C., 1998.

Britter, R. E., and P. F. Linden, The motion of the front of a gravity current travelling down an incline, *J. Fluid Mech.*, *99*, 531–543, 1980.

Condie, S. A., Descent of dense water masses along continental slopes, *J. Mar. Res.*, *53*, 897–928, 1995.

Condie, S. A., and P. B. Rhines, Topographic Hadley cells, *J. Fluid Mech.*, *280*, 349–368, 1994.

Cooper, L. H. N., and D. Vaux, Cascading over the continental slope of water from the Celtic Sea, *J. Mar. Biol. Assoc.U. K.*, *28*, 719–750, 1949.

Cornish, V., *Ocean Waves and Kindred Geophysical Phenomena*, 164 pp., Cambridge Univ. Press, New York, 1934.

Dressler, R. F., Mathematical solution of the problem of roll waves in inclined open channels, *Commun. Pure Appl. Math.*, *2*, 149–194, 1949.

Ellison, T. H., and J. S. Turner, Turbulent entrainment in stratified flows, *J. Fluid Mech.*, *6*, 423–448, 1959.

Fahrbach, E., G. Rohardt, N. Scheele, M. Schröder, V. Strass, and A. Wisotzki, Formation and discharge of deep and bottom water in the northwestern Weddell Sea, *J. Mar. Res.*, *53*, 515–538, 1995.

Farmer, D., and L. Armi, Stratified flow over topography: The role of small-scale entrainment and mixing in flow establishment, *Proc. R. Soc. London, Ser. A*, *455*, 3221–3258, 1999.

Fer, I., Dynamics of winter cooling in Lake Geneva, Ph.D. thesis, 150 pp., Ecole Polytech. Fed. de Lausanne, Lausanne, Switzerland, 2001.

Fer, I., U. Lemmin, S. A. Thorpe, The winter cold slope boundary layer, paper presented at Fifth IAHR International Symposium on Stratified Flows, Int. Assoc. for Hydraul. Res., Vancouver, B. C., Canada, 2000.

Fer, I., U. Lemmin, and S. A. Thorpe, Cascading of water down the sloping sides of a deep lake in winter, *Geophys. Res. Lett.*, *28*, 2093–2096, 2001.

Fer, I., U. Lemmin, and S. A. Thorpe, Observations of mixing near the sides of a deep lake in winter, *Limnol. Oceanogr.*, *47*, 535–544, 2002.

Fischer, H. B., E. J. List, R. C. Y. Koh, J. Imberger, and N. H. Brooks, *Mixing in Inland and Coastal Waters*, 483 pp., Academic, San Diego, Calif., 1979.

Hay, A. E., Turbidity currents and submarine channel formation in Rupert Inlet, British Columbia, part 1, Surge observations, *J. Geophys. Res.*, *92*, 2875–2881, 1987.

Hill, A. E., A. J. Souza, K. Jones, J. H. Simpson, G. I. Shapiro, R. McCandliss, H. Watson, and J. Leftley, The Malin cascade in winter, *J. Mar. Res.*, *56*, 87–116, 1998.

Lane-Serff, G. F., and P. G. Baines, Eddy formation by dense flows on slopes in a rotating fluid, *J. Fluid Mech.*, *363*, 229–252, 1998.

Lane-Serff, G. F., and P. G. Baines, Eddy formation by overflows in stratified water, *J. Phys. Oceanogr.*, *30*, 327–337, 2000.

Muench, R. D., and A. L. Gordon, Circulation and transport of water along the western Weddell Sea margin, *J. Geophys. Res.*, *100*, 18,503–18,515, 1995.

Needham, D. J., and J. H. Merkin, On roll waves down an open inclined channel, *Proc. R. Soc. London, Ser. A*, *394*, 259–278, 1984.

Pedlosky, J., *Geophysical Fluid Dynamics*, 624 pp., Springer-Verlag, New York, 1979.

Phong-Anant, D., R. V. Antonia, A. J. Chambers, and S. J. Rajagopalan, Features of the organized motion in the atmospheric surface layer, *J. Geophys. Res.*, *85*, 424–432, 1980.

Prasad, S. N., D. Pal, and M. J. Romkens, Wave formation on a shallow layer of flowing grains, *J. Fluid Mech.*, *413*, 89–110, 2000.

Shay, T. J., and M. C. Gregg, Convectively driven turbulent mixing in the upper ocean., *J. Phys. Oceanogr.*, *16*, 1777–1798, 1986.

Smith, P. C., Experiments with viscous source flows in rotating systems, *Dyn. Atmos. Ocean*, *1*, 241–272, 1977.

Soloviev, A. V., Coherent structures at the ocean surface in convectively unstable conditions, *Nature*, *346*, 157–160, 1990.

Sturman, J. J., C. E. Oldham, and G. N. Ivey, Steady convective exchange flows down slopes, *Aquat. Sci.*, *61*, 260–278, 1999.

Thorpe, S. A., Small-scale processes in the upper ocean boundary layer, *Nature*, *318*, 519–522, 1985.

Thorpe, S. A., and A. J. Hall, The mixing layer of Loch Ness, *J. Fluid Mech.*, *101*, 687–703, 1980.

Thorpe, S. A., and U. Lemmin, Internal waves and temperature fronts on slopes, *Ann. Geophys.*, *17*, 1227–1234, 1999.

Thorpe, S. A., M. Curé, and M. White, The skewness of temperature derivatives in oceanic boundary layers, *J. Phys. Oceanogr.*, *21*, 428–433, 1991.

Thorpe, S. A., U. Lemmin, C. Perrinjaquet, and I. Fer, Observations of the thermal structure of a lake using a submarine, *Limnol. Oceanogr.*, *44*, 1575–1582, 1999.

Tomczak, M., Bass Strait water cascade during winter 1981, *Cont. Shelf Res.*, *4*, 255–278, 1985.

Turner, J. S., *Buoyancy Effects in Fluids*, 367 pp., Cambridge Univ. Press, New York, 1973.

Whitehead, J. A., M. E. Stern, G. R. Flierl, and B. A. Klinger, Experimental observations of baroclinic eddies on a sloping bottom, *J. Geophys. Res.*, *95*, 9586–9610, 1990.

Zatsepin, A. G., A. G. Kostyanoi, and A. V. Semenov, An axisymmetric density current over a sloping bottom in a rotating fluid, *Oceanology*, *36*, 311–316, 1996.

Zilitinkevich, S. S., K. D. Kreiman, and A. Y. Terzevik, The thermal bar, *J. Fluid Mech.*, *236*, 27–42, 1992.

I. Fer, Geophysical Institute, University of Bergen, Allegaten 70, N-5007 Bergen, Norway. (ilker.fer@gfi.uib.no)

U. Lemmin, LRH, EPFL, CH-1015, Lausanne, Switzerland.

S. A. Thorpe, School of Ocean and Earth Science, Southampton Oceanography Centre, European Way, Southampton SO14 3ZH, UK.